Nanoscale

Effects of length dispersity and film fabrication on the sheet resistance of copper nanowire transparent conductors†

James W. Borchert,[a] Ian E. Stewart,[b] Shengrong Ye,[b] Aaron R. Rathmell,[b] Benjamin J. Wiley[b] and Karen I. Winey*[a]

Development of thin-film transparent conductors (TC) based on percolating networks of metal nanowires has leaped forward in recent years, owing to the improvement of nanowire synthetic methods and modeling efforts by several research groups. While silver nanowires are the first commercially viable iteration of this technology, systems based on copper nanowires are not far behind. Here we present an analysis of TCs composed of copper nanowire networks on sheets of polyethylene terephthalate that have been treated with various oxide-removing post treatments to improve conductivity. A pseudo-2D rod network modeling approach has been modified to include lognormal distributions in length that more closely reflect experimental data collected from the nanowire TCs. In our analysis, we find that the copper nanowire TCs are capable of achieving comparable electrical performance to silver nanowire TCs with similar dimensions. Lastly, we present a method for more accurately determining the nanowire area coverage in a TC over a large area using Rutherford Backscattering Spectrometry (RBS) to directly measure the metal content in the TCs. These developments will aid research and industry groups alike in the characterization of nanowire based TCs.

1. Introduction

Transparent conducting materials are essential to many current electrical devices such as smart phones, EMI shielding, and organic solar cells. Current applications are primarily relegated to flat, non-flexible display technologies. The greatest push for development in TCs is to incorporate flexibility while still retaining the necessary optical and electrical properties. This quality has thus far been unobtainable for the current industry-leading TC material, indium tin oxide (ITO) due to its inherent brittleness. In addition, very high processing costs along with volatility of the supply of indium has further motivated the search for replacement materials for use in TCs.[11,12] A steadily increasing breadth of research continues to demonstrate nanowire networks as the most viable alternative to ITO for these applications.[7] This is due in part to the ability of thin films of nanowire networks to simultaneously achieve low sheet resistance ($R_s < 100\ \Omega\ \mathrm{sq}^{-1}$), high

flexibility, and high optical transparency ($T > 90\%$) at a lower manufacturing cost than ITO.[8] Thin films of solution-synthesized metal nanowires are made from inks that are deposited by various solution-casting methods such as roll-to-roll slot die, spray coating, and spin coating. These fabrication methods are generally more cost effective than the high temperature vapor deposition and vacuum procedures required for ITO.

Silver nanowire (Ag NW) films have shown the greatest promise for these applications with sheet resistances and transparencies on par with or exceeding that of typical ITO films.[9,10,18] Since silver has its own inherent high costs there is additional interest in incorporating other metals such as copper nanowires (Cu NWs), into TC applications in order to further reduce the cost of manufacturing.[11] The average price of silver is 100 times more than copper and copper is 1000 times more abundant[13,14] making it an economically attractive alternative to silver. However, Cu NWs have several obstacles to overcome before their incorporation into TC applications can be realized. Many challenges have recently been addressed and adequately solved including (i) increasing the Cu NW aspect ratio to increase conductivity, (ii) decreasing diameter to increase optical transparency, and (iii) developing solution phase approaches for rendering nanowire networks highly conductive.[11,19–22,27] The propensity of copper to oxidize

[a]Department of Materials Science and Engineering, University of Pennsylvania, Philadelphia, Pennsylvania 19104, USA. E-mail: winey@seas.upenn.edu
[b]Department of Chemistry, Duke University, 124 Science Drive, Box 90354, Durham, North Carolina 27708, USA
†Electronic supplementary information (ESI) available: Contains calibration curve for %*T* vs. area fraction. See DOI: 10.1039/c5nr03671b

results in increasing sheet resistance of TC devices, commonly attributed to the high contact resistance at nanowire–nanowire junctions due to the insulating copper oxide layers coating the nanowires that are clearly visible in TEM examinations of the nanowires.[19,21,22,27] Reliable methods have been developed to remove the oxide surface layer on Cu NWs using either acetic acid washes or plasma cleaning in combination with high temperature hydrogen annealing.[19,22] Sheet resistances nearly on par with that found in sintered Ag NW networks have been achieved by plasma cleaning the Cu NW networks and subsequently annealing in a hydrogen-rich atmosphere after film fabrication.[19] However, the necessity of the hydrogen rich annealing atmosphere and higher temperatures presents a disadvantage in that neither of these are required by Ag NW based TCs. Alternatively, washing the films in acetic acid has proven particularly promising to increase conductivity. For example, networks of Cu NWs with average length $<L>$ = 20 μm and average diameter $<D>$ = 67 nm ($<L>/<D>$ = 300) exhibit a sheet resistance of 50 Ω sq^{-1} a transmittance of 90% when treated with this method.[22] A solution-based post treatment such as the acetic acid wash is likely to be highly preferred relative to a plasma treatment and hydrogen gas annealing.

The full impact of post-treatment on the performance of TCs is difficult to assess, because there are several materials and physical parameters that determine the electrical and optical properties of nanowire-based TCs: nanowire conductivity, nanowire-nanowire contact resistance, nanowire areal coverage, and nanowire dimensions. To quantify the impact of these parameters on electrical conductivity, we previously developed a Monte Carlo simulation method that builds 3D rod networks and then computes the electrical conductivity by approximating that all resistance in the network originated from the nanowire-nanowire contact resistance, R_c.[1–4,6] To address the case of transparent conductors, the model was modified to build pseudo-2D rod networks, where the thickness of the network is equal to the diameter of the rod. By comparing the experimental sheet resistance of well-characterized Ag NW samples the contact resistance was determined.[3] Specifically, experimental sheet resistance data for TCs of various nanowire areal coverage with Ag NWs of modest aspect ratios (L/D = 200–275) and diameters of 50, 75, and 84 nm are in good agreement with the simulations.[3] Moreover, the effective contact resistance between Ag NWs synthesized and fabricated in that manner was found to be 1.5–2.5 kΩ. Longer wires were also shown to increase the electrical conductivity of the network at a fixed area fraction owing to a decrease in the critical percolation threshold.[6] The Ag NWs were assumed to be monodisperse in length and diameter in the model. While current synthetic methods produce nanowires with narrow diameter distributions, the nanowire lengths are polydisperse and typically have a positively skewed distribution towards longer wires.[5,9,15] In this paper, we modify our model to include positively skewed distributions of rod lengths to better represent experimental data. Using the updated version of the model we then assessed the impacts of post treatments on R_c for Cu NW networks deposited on PET.

Several approaches are examined including repeated rinsing of the films in acetic acid,[22] mechanical pressing,[22] and plasma cleaning under forming gas (95% N_2, 5% H_2) and annealing in a hydrogen environment.[19] The Cu NW TCs are shown to have similar R_c values as Ag NW-based TCs with similar dimensions.[3]

Finally, in consideration that these post-treatment methods might remove nanowires from the substrate or alter their optical properties, we have developed a new characterization method for quantifying the area coverage of the nanowire TCs using Rutherford Backscattering Spectrometry (RBS).[16,17] Current techniques exist to measure the projected fractional area coverage of a surface by nanowires, A_F, such as processing many optical or SEM images of the nanowire network using programs like ImageJ or Clemex. This type of method suffers from poor statistics due to limited sampling areas, time-consuming data collection and analysis, and user subjectivity, which leads to limited reproducibility. All of these issues are exacerbated as the nanowire networks are spread over a larger area. A robust method that measures over a large area is necessary for reliable quantification of the area coverage. In one such approach, Bergin et al. found a useful empirical relationship between A_F and the optical transmittance of Ag NW films at λ = 550 nm.[15] While the sample size is improved over the image analysis techniques, this approach could potentially suffer from unwanted changes in the transmittance measurements due to morphology modification of the Cu NW networks or the optical properties of the base substrate. In an effort to get around these issues, we propose that a new method using RBS may be used to measure A_F for a nanowire TC more accurately by taking advantage of the elemental selectivity of RBS. In this approach the measurement of A_F is based on the proportional relationship of the atomic areal density of the nanowires in a TC and the total signal yield attributed to the Cu NWs as measured by RBS.[16,17]

2. Experimental

2.1 Copper nanowire TC films

Cu NWs with an average aspect ratio $<L>/<D>$ = 330 were synthesized using the method described by Rathmell et al.[19] with an average diameter of 76 nm. A modified method described by Ye et al.[21] was used to synthesize Cu NWs with $<L>/<D>$ = 150 and 570 and average diameters of 78 and 64 nm, respectively. Nanowire diameters were measured using a FEI XL 30 SEM-FEG and ImageJ (http://imagej.nih.gov/ij/). Measurements of nanowire lengths were made with an Olympus BX51 optical microscope and the Olympus Stream Image Analysis software. The nanowires were deposited as thin film networks by transferring nanowires dispersed in a nitrocellulose-based ink onto PET using a Meyer rod.[19] The films then received one or more post treatments to remove oxidized layers, reducing the nanowire-nanowire contact resistance, and thereby improving sheet resistance. Post treatments included repeated rinsing

in acetic acid,[22] pressing at room temperature (80 bar, 1 minute),[22] plasma cleaning under a forming gas for 10 minutes, and annealing in a tube furnace under hydrogen gas at 175 °C for 30 minutes.[19] The films were then immediately vacuum sealed and stored in a nitrogen-rich atmosphere until characterization. The average sheet resistance of the Cu NW films determined from 5 measurements in a roughly 2.5 cm × 2.5 cm area with a four-point probe (Signatone S-1160A-5). The probe separation distance for this instrument is 1 mm, significantly greater than the length of the nanowires in each film. The specular transmittance was determined using UV/VIS/NIR measurements (Cary 6000i). A calibration curve (Fig. S1†) for determining A_F was constructed from transmittance measurements of Cu NWs deposited on PDMS *via* the method described by Bergin *et al.*[15]

2.2 Measurement and calculation of area fraction using RBS

Rutherford backscattering spectrometry (RBS) data were collected at normal beam incidence using $^4He^+$ ions accelerated to $E_0 = 2.02$ MeV for each sample. The spot size of the incident beam was set to ~20–30 mm². A passivated implanted planar silicon (PIPS) detector with solid angle $\Omega = 1.59$ msr was placed at an angle $\theta = 170°$ relative to the incident beam. The total collected charge for each sample was 10 μC. Thin films of copper metal were deposited using a thermal evaporator. These films are used as standards for the calculation of area coverage for the copper nanowire TCs. The copper thin films used in this paper are 120–180 nm thick as determined by RBS and AFM measurements.

In RBS measurements, the amount of energy that a backscattered ion loses in the inelastic collisions with the atoms in and on a sample surface depends on the type of incident ion used, the incident energy, the scattering atoms' Z-number, depth within the sample, and the path that the ion takes through the sample before being collected by the detector.[16,17] Several types of scattering events can occur between the incident ion and the atoms in a nanowire TC sample. If the ion scatters off of a copper atom at the surface of one of the nanowires it will lose the smallest amount of energy, corresponding to the front edge of the energy peak in the spectrum (Fig. 1). The tailing of the copper peak to lower backscattering energy is due to scattering from a copper atom that is not on the surface of a wire or secondary collisions with copper atoms after interaction(s) with other atoms in the sample. These latter interactions are what necessitate the use of a copper metal thin film standard in order to calculate A_F. In RBS measurements, the total number of detected particles or yield, Y_i, from an element, i, in a sample is related to the atomic areal density of that element, $(Nt)_i$, by

$$Y_i = \sigma_R(E,\theta)_i \Omega Q (Nt)_i \quad (1)$$

where $\sigma_R(E,\theta)_i$ is the differential backscattering cross section of the element, E is the incident beam energy, θ is the angle at which the detector is placed relative to the beam, Ω is the solid angle subtended by the detector, and Q is the
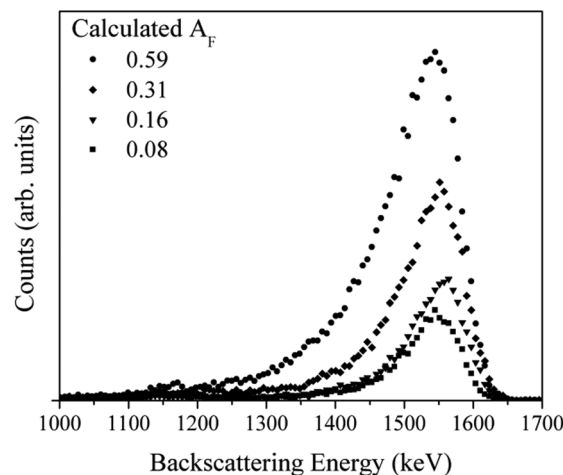

Fig. 1 Representative RBS spectra for Cu nanowire TCs, where the area fractions calculated from the RBS data are given in the legend. Note that the intensity of the copper peak scales with the area fraction as expected.

total number of incident ions or dose. The atomic areal density and subsequently A_F can be determined for the nanowire samples by comparing results from eqn (1) for the nanowire TC and the copper thin film standard. Noting that Ω and Q depend solely on the instrumental setup and, thus, are constant for our experiments, we can solve for the product ΩQ. Next, we solve for the atomic areal density of the element i in the nanowire sample, $(Nt)_i^{NW}$, and obtain an expression for calculating the atomic areal density of copper in the nanowire TC:

$$(Nt)_i^{NW} = \frac{Y_i^{NW}}{Y_i^o} \frac{\sigma_R(\bar{E},\theta)_i^o}{\sigma_R(\bar{E},\theta)_i^{NW}} (Nt)_i^o \quad (2)$$

where the superscript "o" denotes quantities from the copper thin film. All of the terms on the right can be obtained from either RBS data or from the instrumental set up except for the scattering cross sections which must be calculated. For a large θ the scattering cross section, σ_R, can be approximated by

$$\sigma_R(E,\theta) \cong 0.02073 \left[\frac{Z_1 Z_2}{4E}\right]^2 \left[\sin^{-4}\left(\frac{\theta}{2}\right) - 2\left(\frac{M_1}{M_2}\right)^2\right] \quad (3)$$

where Z_1 and M_1 are the atomic number and mass for the incident particles, respectively, and Z_2 and M_2 are for the target atoms. For the nanowire samples we can simply use the incident energy, E_0, for the calculation of the scattering cross section since the vast majority of scattering events are close to the surface. For thin films, we need to account for additional energy losses that are dependent on the thickness of the calibration film. In the so-called surface energy approximation, SEA, we calculate the mean energy, $\bar{E}$, to a first approximation within the film and use this quantity when calculating the cross section.

$$\bar{E} = E_0 - \frac{\Delta E_{in}^{SEA}}{2} \quad (4)$$

where the energy loss is calculated from data by

$$\Delta E_{in}^{SEA} = \varepsilon^i(E_0)(Nt)_i \tag{5}$$

The stopping cross section of the target element, ε^i, is tabulated. We can now readily calculate $(Nt)_i^{NW}$ for each nanowire TC from RBS data. From this quantity A_F is calculated assuming that all nanowires can be modeled as cylinders with constant diameter D which is taken to be the experimentally obtained average diameter. The junctions where nanowires cross are double counted in our calculation. However, this additional contribution is negligible in the overall calculation of the area fraction for high aspect ratio wires near the percolation threshold. The number of atoms per unit volume is considered to be equivalent to the bulk atomic density of the material, ρ_B. The fraction of the surface area of a TC covered by nanowires, A_F, is directly proportional to the atomic areal density and the dimensions, $<L>$ and $<D>$, and inversely proportional to the number of atoms per wire, n, which is calculated using ρ_B, the volume of a wire, and the molecular weight of the nanowire component element, M_i.

$$n = \frac{\pi \rho_B D^2 L}{4 M_i} \tag{6}$$

Substitution leads to the expression for calculating the area fraction from the atomic areal density measured by RBS for a nanowire TC:

$$A_F = \frac{4(Nt)_i^{NW} M_i}{\pi \rho_B D} \tag{7}$$

2.3 Application of length distributions to simulations

Our Monte Carlo method for pseudo-2D rod networks was previously described.[1–4] In brief, a nanowire network deposited on a flat substrate is represented by a network of isotropically-oriented, interpenetrating cylindrical rods confined to the x–y plane of a supercell with dimensions $1 \times 1 \times D_{rod}$, where D_{rod} is the diameter of an individual rod (typically $D_{rod} = 10^{-5}$ to 10^{-4} a.u.). The internal resistance of the rods is assumed to be zero while the resistance of the surrounding medium is infinite. Therefore all resistance in the network of rods is attributed to a single effective contact resistance, R_c, applied to each of the rod–rod intersections. This is understood to be the average contact resistance between wires in the TC.

Distributions of rod lengths to be used in the simulations were determined by fitting experimental measurements of nanowire lengths with a lognormal distribution (Fig. 2). The fit routine followed the form

$$f(L) = A + \frac{B}{\sigma L \sqrt{2\pi}} e^{-\frac{\ln\left(\frac{L}{<L>}\right)^2}{2\sigma^2}} \tag{8}$$

where the constants A and B are fitting parameters. The best fitting distribution with average length $<L>$ and standard deviation σ was then applied to the rods in the simulation *via* the lognormal random number generator function from the GNU Scientific Library. To verify that the proper distributions were
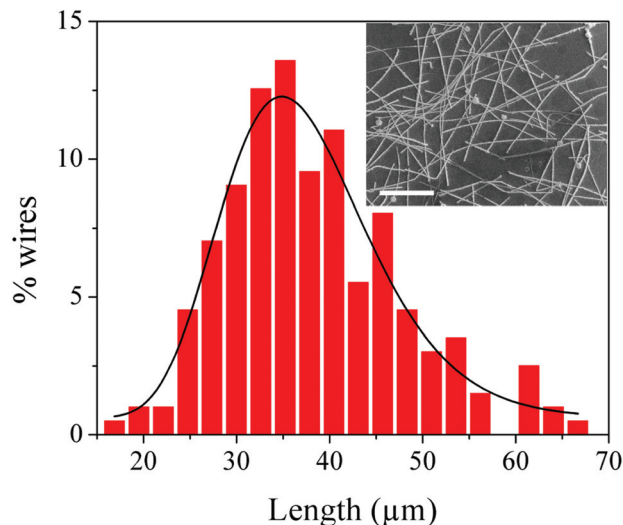

Fig. 2 Histogram of Cu NW lengths as measured by SEM. The distribution of lengths is fit with a lognormal distribution (black curve) with a mean length of 36.5 μm and a standard deviation of $\sigma = 0.22$. Inset: SEM image of Cu NWs deposited on a PET substrate; scale bar is 10 μm.

being produced, the lengths of the rods used in the simulation were fit using the same lognormal routine and compared with the parameters set in the simulation (Fig. 3a).

3. Results and discussion

3.1 Effect of length polydispersity on sheet resistance

Before combining experimental and simulation results, we examine the impact of rod length dispersity on sheet resistance and percolation threshold. Fig. 3a shows three distributions in rod length where the points are the lengths of rods used in the simulations and the fitted curves are lognormal distributions. The rods have constant D, constant $<L>/D$ and varying standard deviation to give varying degrees of dispersity. The sheet resistance of pseudo-2D rod networks made from rods with these length distributions decreases with increasing length dispersity (Fig. 3b). For example, across the range of area fractions tested a high lognormal dispersity ($\sigma = 0.50$) decreases the sheet resistance by ~50% relative to a low level of dispersity ($\sigma = 0.05$). This result is consistent with longer rods being more effective in constructing a percolated network. Experimentally, typical Cu NWs have measured length dispersity of ~0.20, such that at a fixed areal coverage the reduction of the sheet resistance relative to monodisperse nanowires of the same average length is ~20%. The critical area fraction for percolation, A_C, was extracted from the simulations *via* fitting the conductivity values from the simulations using the relationship
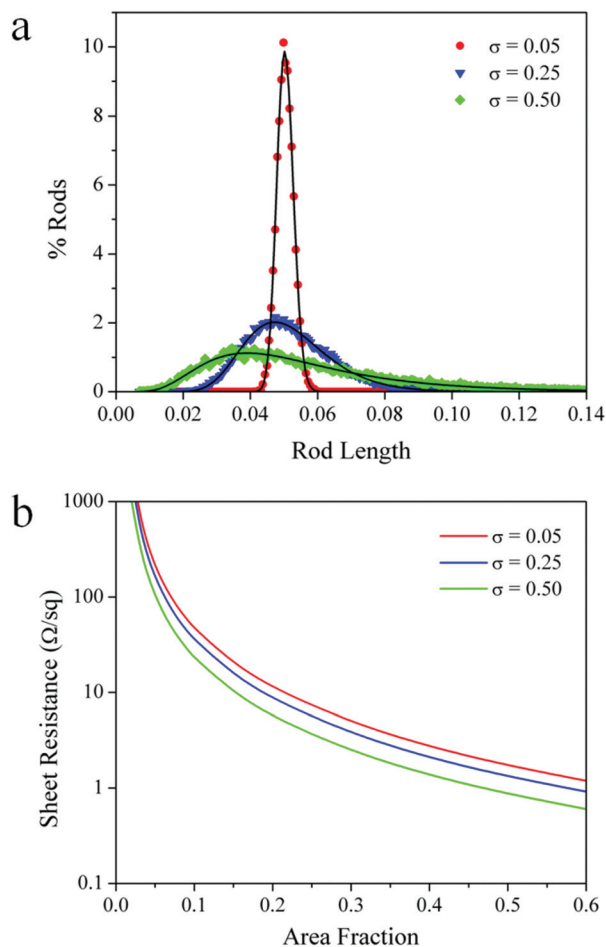
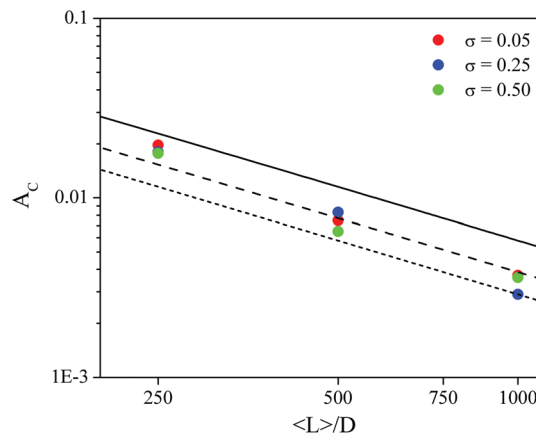$$\sigma = s\left(\frac{A_F - A_C}{A_C}\right)^t \tag{9}$$

Fig. 4 The percolation threshold, A_C, of simulations of networks of rods with varying levels of polydispersity according to lognormal distributions is presented (points). The calculated curves for the percolation threshold of polydisperse networks according to eqn (10) are compared to the values from simulation. The solid line represents the monodisperse case with $<L>_w/<L> = 1$ along with polydisperse cases $<L>_w/<L> = 1.5$ (long dashes) and $<L>_w/<L> = 2$ (short dashes).

Fig. 3 (a) Distributions of rod lengths produced when applying the lognormal distribution in our simulations for the specific case of $A_F = 0.10$, $D = 0.0001$ a.u., $<L>/D = 500$, ~17 000 rods per distribution. Three standard deviations for the lognormal are shown: 0.05, 0.25, and 0.50. As the standard deviation decreases, the distribution approaches that of the monodisperse case where all rods have $L = <L> = 0.05$ a.u. (b) Calculated sheet resistance versus area fraction for $D = 75$ nm corresponding to the three distributions shown in part (a).

where s is simply a scalar. Here we are fitting over $A_F = 0.01–0.60$ which yields higher than universal values for the percolation exponent, t, which varied from 1.8 to 2.[4] In Fig. 3 we show the values for A_C extracted from simulations at three $<L>/D$ with varying levels of polydispersity. As expected, A_C decreases significantly as a function of the aspect ratio, $<L>/D$.[4] However, A_C has a weak dependence on the length polydispersity related to the increase in the weighted average length, $<L>_w$, with σ, as was found by others previously.[23–26] The critical area fraction of a polydisperse system, A_{C_poly}, is given by

$$A_{C\_poly} = \frac{3.7}{\left(2 + \frac{8}{\pi^2}\right) + \left(\frac{\langle L \rangle_w}{D} + \frac{D}{\langle L \rangle}\right)\frac{2}{\pi}} \quad (10)$$

Here we hold the excluded volume to the value of 3.7 and D is constant.[4] At high aspect ratios this relationship is domi-

nated by the weight average term. In the mean field approximation[22] the system is monodisperse when $<L>_w/<L> = 1$ (solid line in Fig. 4). As the system becomes more polydisperse this ratio increases and thereby decreases the percolation threshold for a given $<L>/D$; Fig. 4 shows the results from eqn (10) for $<L>_w/<L> = 1.5$ (long dashes) and 2 (short dashes). In comparison, the simulations exhibit a distinct lack of sensitivity to the level of dispersity across this range of $<L>/D$. This is comparable with previous findings for simulations of 3D rod networks that A_C is insensitive to polydispersity for narrow Gaussian distributions where the standard deviation is <30%.[2] It is interesting that as the aspect ratio increases, the further the simulated data deviates from monodisperse behavior. This again highlights the significant impact of longer rods on percolation.

3.2 Area coverage of nanowire networks in TCs

The nanowire dimensions and areal coverage must be determined in order to apply the simulations of sheet resistance to experimental data and extract the effective contact resistance between Cu NWs. Measurements of D yield a very tight distribution for all the nanowires in this study. Therefore, D is measured for each nanowire batch and held constant in their respective simulations. As illustrated in Fig. 1, the Cu NWs have positively skewed lengths. For each batch of nanowires a lognormal fit is applied to determine the mean length, $<L>$, and standard deviation, σ. These nanowire size characteristics (D, $<L>$, σ) are then incorporated into the simulations to give a more accurate representation of the real nanowire network.

The number of rods in the simulations is set by the areal coverage of nanowires as determined by our RBS method. RBS is widely used in the electronics industry to characterize the composition of thin films and the dopant concentration in silicon. Fig. 1 shows RBS data for Cu NW films on PET sub-
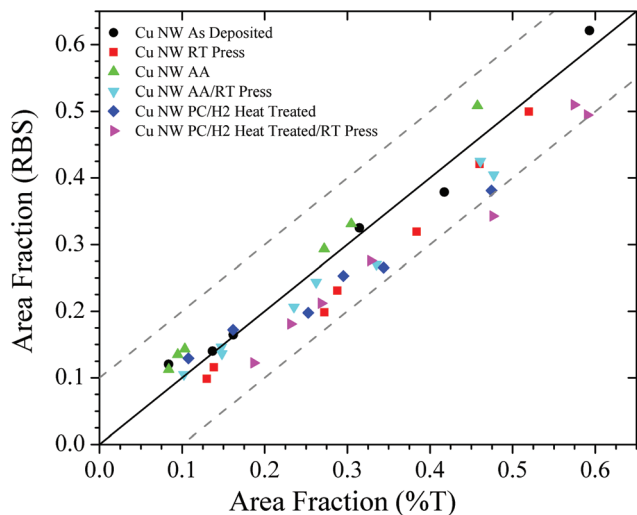
Fig. 5 Comparison of area fractions measured using RBS *versus* area fractions obtained through transmission measurements (%T). Cu nanowires have an average aspect ratio $\langle L \rangle / \langle D \rangle$ = 330. Post treatment nomenclature: AA: acetic acid washed four times; RT Press: pressed 80 bar for 1 minute at room temperature; PC/H_2: plasma cleaned under forming gas and then annealed in H_2 rich environment at 175 °C for 30 minutes. The dotted lines denote a $\pm$10% deviation from perfect agreement between the two methods (solid line).

Fig. 6 Sheet resistance as a function of area fraction from Cu NW networks deposited on PET (points) and from simulations (solid line R_c = 2 kΩ, dashed line R_c = 1 kΩ). Four post-treatments were applied using one or more of the following as indicated in the legends: AA: acetic acid washed four times, RT Press: pressed 80 bar for 1 minute at room temperature, PC/H_2: plasma cleaned under forming gas and then annealed in a hydrogen rich environment at 175 °C for 30 minutes. Simulations use rod dimensions determined by SEM and fit with a lognormal distribution (D = 76 nm, $\langle L \rangle$ = 330 nm, σ = 0.20).

strates wherein the area under the curve in the counts *versus* energy plot increases with the copper content. The Cu nanowire TCs were found to have area fractions ranging between 0.08 and 0.59. These A_F values and those obtained from the optical transmittance method[14] show good agreement (Fig. 5) with less than 10% variation between the two methods in most cases. Notably, the measurements from the as-deposited Cu NWs (no post-treatments) show the greatest level of agreement, while the post-treated TCs tend to deviate from RBS-measured values.

The samples that were both plasma cleaned and pressed at room temperature showed the highest deviations. The optical transmission measurements apparently overestimate the area fraction in these samples. It may be due to the non-selectivity of the optical transmission method which is sensitive to contaminants left on the surface after post treatment that may scatter or absorb light. In contrast, RBS measures the copper content directly and is insensitive to the changes in nanowire shape, contaminates, and residues. These data clearly demonstrate the feasibility of RBS to quantify areal coverage before and after post-processing without the ambiguities associated with relating optical transparency to nanowire coverage. Further, the RBS spot size is ~1 mm, so lateral uniformity of a NW film can be quantified. Area fractions of the nanowire TC reported in the remainder of this paper are measured with the RBS method.

3.3 Effects of post-processing on network conductivity

Fig. 6 shows the measured sheet resistance for TC films on PET made with Cu NWs with $\langle L \rangle / D$ = 330 and D = 76 nm that
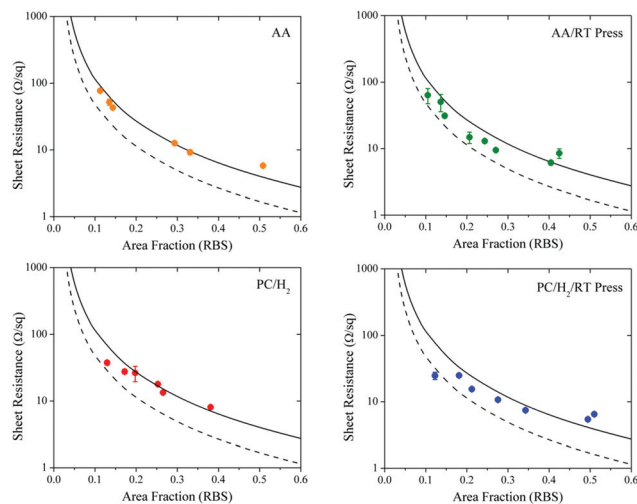
underwent various post treatments. Note that Cu NW films with no post treatment or with only room temperature mechanical pressing are very highly insulating due to poor electrical contact primarily from the copper oxides present on the NWs. Although the mechanical pressing technique enhances contact between the nanowires, it is still oxide to oxide contact, so oxide reduction methods are required for significant increases in the conductivity of the network. The acetic acid washes and plasma cleaning plus annealing approaches to reduce the contact resistance improve the conductivity of the films dramatically. When oxide removal measures were followed by room temperature pressing, the sheet resistances decreased slightly for area fractions <0.4 and showed no change at higher area fractions. This is attributed to the scenario at low A_F where there are fewer nanowire-nanowire contacts, such that even relatively small improvements in contact resistance between nanowires like that provided from pressing can have a significant effect on electrical percolation behavior of the TC.

To quantify this comparison between post-processing methods R_c values were extracted by fitting the experimental sheet resistance *versus* A_F experimental data with a simulated curve using the D, $\langle L \rangle$, and σ for these nanowires and A_F determined by RBS. The four post treatments produce Cu NW networks that have similar effective contact resistances of ~1–2 kΩ. Notably, this is similar to the contact resistance range of 1.5–2.5 kΩ that was determined for Ag NW films composed of nanowires having diameters of 50, 84, and 75 nm, corresponding to nanowires with L/D = 200, 258, and 275, respectively.[2] This provides further and compelling evidence that
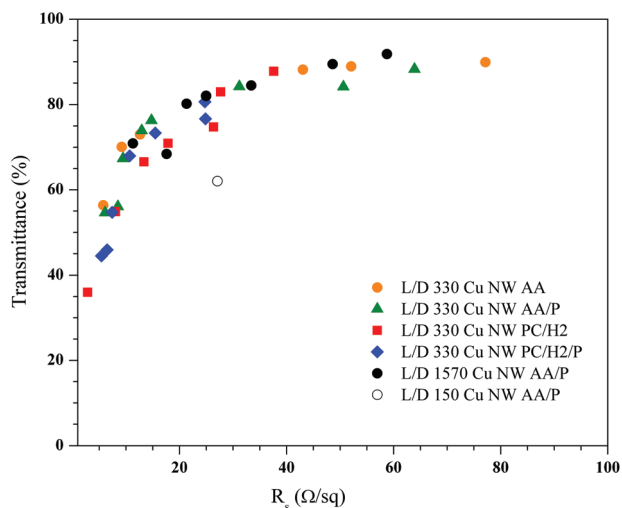
Fig. 7 Transmittance as a function of average sheet resistance for each of the Cu NW networks in this study. AA: acetic acid washed four times, RT Press: pressed 80 bar for 1 minute at room temperature, PC/H$_2$: plasma cleaned under forming gas and then annealed in a hydrogen rich environment at 175 °C for 30 minutes.

networks of Cu NWs can achieve similar levels of conductivity as networks composed of Ag NWs with comparable dimensions as long as steps are taken to remove oxides. Moreover, given the similarities of the sheet resistances and the optical performance after the four post treatments (Fig. 7), it is clear that the acetic acid treatment can replace the more expensive methods involving plasma cleaning and annealing in a hydrogen-rich environment.[22]

3.4 Further model refinements

To date we have evaluated our pseudo-2D network simulations using experimental systems with aspect ratios of ~200–500 and found good agreement. Outside of this range there are deviations that must be addressed. Fig. 8a compares simulations and experiments with Cu NWs of $<L>/D = 150$ using a post treatment of plasma cleaning and annealing in a hydrogen rich environment. The model estimates an upper bound for the effective contact resistance of $R_C = 500$ kΩ at the lowest area fraction and a lower bound of $R_C = 2$ kΩ for the highest area fraction samples. By inspection of the experimental data, the critical area fraction appears to be higher ($A_C \sim 0.20$) than predicted in either of the simulations. This may be caused by experimental difficulties in distributing the shorter nanowires into a well-dispersed film at low area fractions. At higher loadings, aggregation of the Cu NWs would be less impactful on the sheet resistance of the network. This explanation may help to explain the apparent approach to the $R_C = 2$ kΩ curve at higher A_F. In addition, the predicted number of junctions would be higher than what is actually present in the sample since shorter, less flexible nanowires may not form strong junctions with other wires they are contacting. The simulations could be further refined to address the impact of poor dispersion on the percolation behavior of the networks.
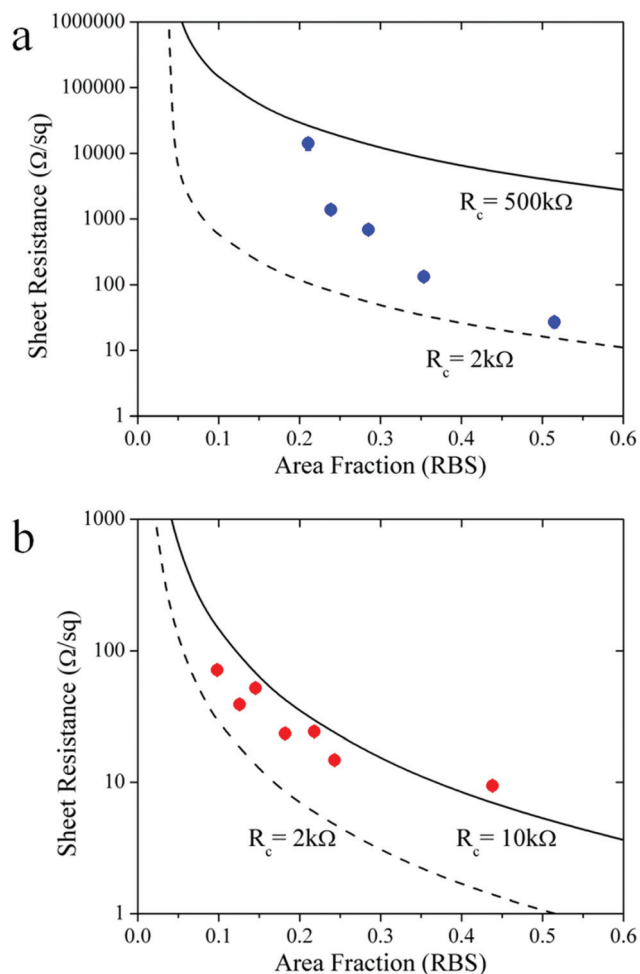

Fig. 8 Experimental (points) and simulated (lines) sheet resistance data as a function of area fraction. Cu NWs were deposited on PET and plasma cleaned under forming gas and then annealed in a hydrogen rich environment at 175 °C for 30 minutes. Simulations used mean diameter and lognormal length distributions consistent with the experiments. (a) $<D> = 78$ nm, $<L>/D = 150$, $\sigma = 0.20$. (b) $<D> = 64$ nm, $<L>/D = 570$, $\sigma = 0.23$. Simulations were performed with two contact resistances, R_c, that establish an upper and lower limit of R_c relative to the experimental sheet resistances.

Cu NWs with $<L>/D = 570$ treated with plasma cleaning and annealing in hydrogen show better agreement between simulations and experiment (Fig. 8b). The extracted contact resistance in this case is $R_C \sim 2$–10 kΩ, which is somewhat higher than the Cu NWs with lower aspect ratios (Fig. 6). The higher contact resistance could be associated with the higher aspect ratio of these wires. Note that the simulations assume that the resistance of the nanowires is negligible and that network sheet resistance arises from the resistance of the contacts alone. However, with increasing aspect ratio the average distance between nanowire–nanowire contacts increases, so that the contribution from the nanowire resistance becomes more important. By neglecting the nanowire resistance, the contact resistance extracted from our simulations is likely a convolution of both the actual contact resistance between nanowires

and the resistance of the nanowires themselves. Modifying the simulations to include the nanowire resistance is likely a necessary refinement of the model and will become increasingly important as nanowire aspect ratios continue to increase.

4.   Conclusions

Transparent conducting films have been made from percolating Cu NW networks that received various post treatments to improve sheet resistance. Specifically, the processing steps were designed to remove the copper oxide layer on the nanowires and thereby reduce the contact resistance between nanowires. To quantify the impact of these processing steps we modified our previously developed Monte Carlo model of pseudo-2D rod networks[2] to include length polydispersity using lognormal distributions. We find that length dispersities of ~0.20 lead to a ~20% reduction of the sheet resistance relative to monodisperse nanowires with the same average length. The simulations show that even modest length dispersity impacts sheet resistance. These results highlight the importance of controlling both the average length and the length dispersity to produce TCs with consistent sheet resistances. Additional refinements to this model could incorporate nanowire resistance, nanowire stiffness, distributions of contact resistance, and sample heterogeneities. Experimental work on these material characteristics of Cu NWs would be beneficial to further improving simulations.

Our simulations are in good agreement with experimental sheet resistance data from Cu NWs with modest aspect ratios of $<L>/D$ = 330 and 570 that underwent oxide removing post treatments. For the former we extract an effective contact resistance of ~2 kΩ, on par with the value extracted for Ag NWs with similar dimensions.[10] Comparable contact resistances were obtained using a plasma cleaning step followed by annealing in a hydrogen-rich environment and the simpler method involving washing with acetic acid and drying. These results provide additional evidence that Cu NWs could represent a more cost-effective alternative to Ag NWs in transparent conducting applications.

In addition, we presented a newly developed method to determine the areal coverage of nanowires using RBS that is more accurate than optical transmission approaches, especially for networks that have received post treatments to improve conductivity. This RBS method is also faster than imaging methods and equally capable of analyzing the areal density of Ag nanowires. There are many facilities capable of performing these measurements for companies and university groups investigating the use of metal nanowires in transparent conductors.

Acknowledgements

References

1 S. I. White, B. A. DiDonna, M. Mu, T. C. Lubensky and K. I. Winey, *Phys. Rev. B: Condens. Matter*, 2009, **79**, 024301.

2 R. M. Mutiso, M. C. Sherrott, J. Li and K. I. Winey, *Phys. Rev. B: Condens. Matter*, 2012, **86**, 214306.

3 R. M. Mutiso, M. C. Sherrott, A. R. Rathmell, B. Wiley and K. I. Winey, *ACS Nano*, 2013, 7, 7654–7663.

4 S. I. White, R. M. Mutiso, P. M. Vora, D. Jahnke, S. Hsu, J. M. Kikkawa, J. Li, J. E. Fischer and K. I. Winey, *Adv. Funct. Mater.*, 2010, **20**, 2709–2716.

5 J.-Y. Lee, S. T. Connor, Y. Cui and P. Peumans, *Nano Lett.*, 2008, **8**, 689–692.

6 R. M. Mutiso and K. I. Winey, *Phys. Rev. E: Stat. Phys., Plasmas, Fluids, Relat. Interdiscip. Top.*, 2013, **88**, 032134.

7 D. Langley, G. Giusti, C. Mayousse, C. Celle, D. Bellet and J.-P. Simonato, *Nanotechnology*, 2013, **24**, 452001.

8 S. Ye, A. R. Rathmell, Z. Chen, I. E. Stewart and B. J. Wiley, *Adv. Mater.*, 2014, **26**, 6670–6687.

9 S. De, T. M. Higgins, P. E. Lyons, E. M. Doherty, P. N. Niermalraj, W. J. Blau, J. J. Boland and J. N. Coleman, *ACS Nano*, 2009, **3**, 1767–1774.

10 M. Song, D. S. You, K. Lim, S. Park, S. Jung, C. S. Kim, D.-H. Kim, D.-G. Kim, J.-K. Kim, J. Park, Y.-C. Kang, J. Heo, S.-H. Jin, J. H. Park and J.-W. Kang, *Adv. Funct. Mater.*, 2013, **23**, 4177–4184.

11 A. R. Rathmell, S. M. Bergin, Y.-L. Hua, Z.-Y. Li and B. J. Wiley, *Adv. Mater.*, 2010, **22**, 3558–3563.

12 U. S. Geological Survey, *Mineral Commodity Summaries, Indium*, U.S. Department of the Interior, Washington, 2014, p. 74.

13 U. S. Geological Survey, *Mineral Commodity Summaries, Silver*, U.S. Department of the Interior, Washington, 2014, p. 146.

14 U. S. Geological Survey, *Mineral Commodity Summaries, Copper*, U.S. Department of the Interior, Washington, 2014, p. 48.

15 S. M. Bergin, Y.-H. Chen, A. R. Rathmell, P. Charbonneau, Z.-Y. Li and B. J. Wiley, *Nanoscale*, 2012, **4**, 1996–2004.

16 L. C. Feldman and J. W. Mayer, *Fundamentals of surface and thin film analysis*, North-Holland, 1986.

17 J. R. Tesmer and M. A. Nastasi, *Handbook of modern ion beam materials analysis*, Materials Research Society, 1995.

18 G. Khanarian, J. Joo, X.-Q. Liu, P. Eastman, D. Werner, K. O'Connell and P. Trefonas, *J. Appl. Phys.*, 2013, **114**, 024302.

19 A. R. Rathmell and B. J. Wiley, *Adv. Mater.*, 2011, **23**, 4798–4803.

20 Z. Chen, S. Ye, A. R. Wilson, Y.-C. Ha and B. J. Wiley, *Energy Environ. Sci.*, 2014, **7**, 1461–1467.

21 S. Ye, A. R. Rathmell, I. E. Stewart, Y.-C. Ha, A. R. Wilson, Z. Chen and B. J. Wiley, *Chem. Commun.*, 2014, **50**, 2561–2564.

22 I. E. Stewart, A. R. Rathmell, L. Yan, S. Ye, P. F. Flowers, W. You and B. J. Wiley, *Nanoscale*, 2014, **6**, 5980–5988.

23 A. P. Chatterjee, *J. Chem. Phys.*, 2010, **132**, 224905.

24 A. P. Chatterjee, *J. Stat. Phys.*, 2012, **146**, 244.

25 A. P. Chatterjee, *J. Chem. Phys.*, 2012, **137**, 134903.

26 A. P. Chatterjee, *J. Chem. Phys.*, 2014, **140**, 204911.

27 C. Mayousse, C. Celle, A. Carella and J. P. Simonato, *Nano Res.*, 2014, **7**, 315–324.